Estimation theory of photon-magnon coupling strength in a driven-dissipative double-cavity-magnon system

Jia-Xin Peng,[1,2] Baiqiang Zhu,[1,2] Weiping Zhang,[2,3,4,5] and Keye Zhang[1,2,*]

[1]*Quantum Institute for Light and Atoms, State Key Laboratory of Precision Spectroscopy, Department of Physics, School of Physics and Electronic Science, East China Normal University, Shanghai 200062, China*

[2]*Shanghai Branch, Hefei National Laboratory, Shanghai 201315, China*

[3]*School of Physics and Astronomy, and Tsung-Dao Lee Institute, Shanghai Jiao Tong University, Shanghai 200240, China*

[4]*Shanghai Research Center for Quantum Sciences, Shanghai 201315, China*

[5]*Collaborative Innovation Center of Extreme Optics, Shanxi University, Taiyuan, Shanxi 030006, China*

(Received 9 October 2023; accepted 11 January 2024; published 2 February 2024)

Cavity-magnon systems are emerging as a fruitful architecture for the integration of quantum technologies and spintronic technologies, where magnons are coupled to microwave photons via the magnetic-dipole interaction. Controllable, the photon-magnon (P-M) couplings provide a powerful means of accessing and manipulating quantum states in such hybrid systems. Thus, determining the relevant P-M couplings is a fundamental task. Here we address the quantum estimation problem for the P-M coupling strength in a double-cavity-magnon system with drive and dissipation. The effects of various physical factors on the estimation precision are investigated and the underlying physical mechanisms are discussed in detail. Considering that in practical experiments it is almost infeasible to perform measurements on the global quantum state of this composite system, we identify the optimal subsystem for performing measurements and estimations. Further, we evaluate the performance of different Gaussian measurements, indicating that optimal Gaussian measurement almost saturates the ultimate theoretical bound on the estimation precision given by the quantum Fisher information.

DOI: 10.1103/PhysRevA.109.022601

I. INTRODUCTION

In the field of quantum optics, the electric-dipole interaction of electromagnetic fields with matter is widely studied, while the magnetic-dipole interaction is often neglected [1,2]. This is because in most cases, the electric-dipole interaction is much stronger than the magnetic-dipole one. However, when electromagnetic fields interact with magnetic materials with very high electron spin density, the magnetic-dipole interaction dominates [3]. Yttrium iron garnet (YIG) crystals, a class of ferrimagnetic materials with low-loss and high-spin density, have attracted much attention in recent years [4–7]. In particular, the magnon modes excited in YIG crystals and microwave photons can realize the cavity-magnon polaritons and the vacuum Rabi splitting [8,9], which induced the creation of cavity-magnon systems that brought quantum optics and magnetism researchers together to develop the integration of quantum physics and spintronic technologies [4].

The photon-magnon (P-M) coupling induced by the magnetic-dipole interaction in the cavity-magnon system links some of the most exciting concepts in modern physics and has been experimentally implemented [4–6]. More recently, many interesting quantum effects have been studied based on such hybrid systems, including the magnon-photon (magnon) entanglement [10–14], magnon chaos [15,16], magnon blocking [17,18], magnon-induced transparency [19–21], bistability [22–24], and Kerr effect [20,25,26], to name a few. Importantly, these phenomena are closely related to the magnetic-dipole interaction strength. A recent review article compared the cavity-magnon systems of different structures, giving different ranges of values for their P-M coupling strengths [4]. From a theoretical viewpoint, grasping the P-M coupling requires simultaneous solving of Maxwell's equations and the Landau-Lifshitz-Gilbert equation [4,27]. Additionally, exploring the P-M coupling is also key to building hybrid cavity-magnon systems for quantum communication technology and realizing potential docking with quantum information science. Consequently, accurate knowledge of the P-M coupling strength is an essential task, extremely important both for understanding magnetic-dipole interaction and for technical applications, and determines the depth of exploration in the cavity-magnonics field. However, the direct measurement of P-M coupling strength is a huge challenge, costly and even impossible to achieve. A wise choice is to indirectly estimate the P-M coupling strength from experimental data on other readily measurable observables, i.e., by resorting to the quantum estimation theory (QET) [28–30]. Particularly, this idea has been applied for the estimating coupling strength both for light-matter interactions (Rabi frequency) [31–36] and optomechanical systems [37–43].

In recent years, the double-cavity systems have received increasing attention because the auxiliary cavity can facilitate the enhancement or realization of some quantum effects. Examples include facilitating optomechanical ground-state

*kyzhang@phy.ecnu.edu.cn

cooling in the unresolved-sideband regime [44], enabling phonon detection in the optomechanical weak coupling regime, and constructing $\mathcal{PT}$-symmetric systems such as balanced gain-loss coupled cavities [45,46]. It is worth noting that some researchers have also integrated double-cavity system with YIG sphere recently, indicating that the auxiliary cavity can enhance the cavity-magnon quantum correlation [47–50], realize nonreciprocal amplification [51], and controllable quantum phase transition [52]. Naturally, a reasonable prediction is that the auxiliary cavity might be able to assist the parameter estimation task under some conditions.

With such motivations in mind, in this work, we exploit the quantum Fisher information (QFI) [53,54] and classical Fisher information (CFI) [28] to investigate the estimation precision limits and measurement strategy of the P-M coupling strength in a driven-dissipative double-cavity-magnon system, where the primary cavity mode is individually coupled to magnon and an auxiliary cavity mode. We explore the effect of various factors such as temperature, loss rate, driving power, and detuning on the estimation precision limit. Remarkably, in comparison with the auxiliary cavity unassisted case, we find that the estimation precision can be greatly improved by appropriately designing the photon tunneling rate. Moreover, selecting appropriate Kerr nonlinear coefficients of the magnon can also reduce estimation errors and facilitate parameter estimation tasks. Although the fingerprint of the P-M coupling strength is left in the global state of the system, in practical measurements it is almost impossible to access the entire system. To this end, we also investigated how the information about the P-M coupling is distributed in each subsystem. The results show that within most of the given parameter regimes, the primary cavity mode is the optimal subsystem for estimating the P-M coupling strength. Further, we considered performing practically Gaussian measurements on it, exploring how much information about the P-M coupling strength can be experimentally extracted.

This paper is organized as follows. In Sec. II, we introduce the driven-dissipative double-cavity-magnon system used to estimate the P-M coupling strength and its steady-state and quantum fluctuations are then derived by the quantum master equation. In Sec. III, we numerically examine the influence of various factors on the estimation error and identify the optimal subsystem for estimating the P-M coupling parameter, and further explore the performance of several Gaussian measurement strategies. The last section discusses the feasibility of the experiment and concludes this article. In Appendix A, the P-M coupling interaction between the magnons and microwave photons is derived. The stability conditions of the system are given in Appendix B. In Appendix C, we briefly review some basic formalism about the parameter estimation of Gaussian states, including QFI calculations for Gaussian states and the form of CFI under several Gaussian measurements. Appendix D provides the normal mode picture of the system.

II. THEORETICAL MODEL AND DYNAMICAL ANALYSIS

A. The model

The double-cavity-magnon system we proposed, sketched in Fig. 1, consists of a highly polished micrometer-scale YIG

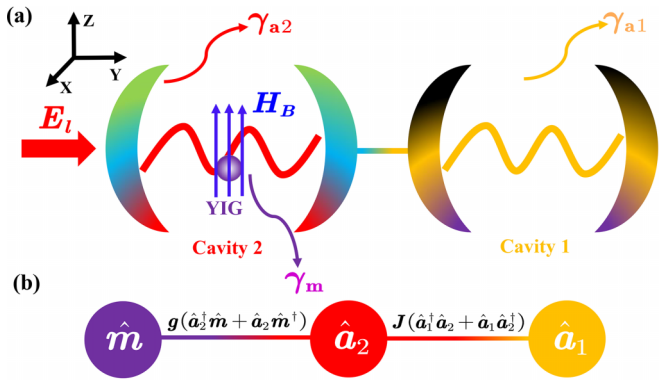

FIG. 1. (a) Diagrammatic representation of the driven-dissipative double-cavity-magnon system. The cavity 2 is driven by a left incident microwave field. Two cavity modes are coupled through photon tunneling. The YIG sphere in the cavity 2 is magnetized to saturation by an external bias magnetic field H_B aligned along the Z direction, which results in the excited magnon modes in the YIG sphere coupled to the cavity modes 2 via the P-M coupling interaction. (b) The diagram of interactions among subsystems in such a hybrid cavity-magnon system.

sphere and two three-dimensional (3D) copper microwave cavities, where the YIG sphere is trapped in the primary cavity 2 and the cavity 1 serves as an auxiliary cavity. The two cavity modes are coupled to each other by a photon tunneling interaction with a hopping rate J. In realistic systems, it can be realized through optical backscattering, which depends on the material defects and surface roughness in experimental devices [55]. Under the action of external static-uniform bias magnetic field H_B along the Z axis, the YIG sphere will excite many magnons, and the magnon modes exhibit uniform spin precession in the YIG sphere [4–6]. At the same time, the Kerr nonlinear effect of the magnons is also induced owing to the magnetocrystalline anisotropy [4–6]. In addition, the magnon mode will couple with the cavity mode 2 via the beam-splitter-like P-M coupling with coupling strength g.

Here, the P-M coupling rate g is the physical parameter we are interested in, i.e., the parameter to be estimated. We consider a microwave field along the Y axis with the power P_l and the frequency ω_l to directly drive the cavity 2. As such, the total Hamiltonian of the hybrid cavity-magnon system can be written as [5,6] (we set $\hbar = 1$ hereafter)

$$\begin{aligned}\hat{H} &= \omega_{a_1}\hat{a}_1^\dagger\hat{a}_1 + \omega_{a_2}\hat{a}_2^\dagger\hat{a}_2 + \omega_m\hat{m}^\dagger\hat{m} + K\hat{m}^\dagger\hat{m}\hat{m}^\dagger\hat{m} \\ &\quad + J(\hat{a}_1^\dagger\hat{a}_2 + \hat{a}_1\hat{a}_2^\dagger) + g(\hat{a}_2^\dagger\hat{m} + \hat{a}_2\hat{m}^\dagger) \\ &\quad + iE_l(\hat{a}_2^\dagger e^{-i\omega_l t} - \hat{a}_2 e^{i\omega_l t}),\end{aligned} \tag{1}$$

where $\hat{a}_1^\dagger$ ($\hat{a}_2^\dagger$) and $\hat{a}_1$ ($\hat{a}_2$) denote the bosonic creation and annihilation operators for the two cavity modes with frequency ω_{a_1} and ω_{a_2}, respectively. $\hat{m}^\dagger$ ($\hat{m}$) being the creation (annihilation) operator for the magnon mode with frequency $\omega_m = \gamma_e H_B - 2\mu_0 K_{\rm an}\gamma_e^2 S/V_m M_b^2$ [4–6], here $\gamma_e/2\pi = 28$ GHz/T is the gyromagnetic ratio for electron (for other parameters see Appendix A). The fourth item refers to the magnon Kerr effect with Kerr nonlinear coefficient K. The fifth and sixth items refer to the photon-photon hopping and the P-M (magnetic-dipole) interaction, respectively. The last term represents the

driving to the cavity mode 2 by the microwave field. $E_l = \sqrt{\gamma_{a_2} P_l/\omega_l}$ being the amplitude of driving field, in which γ_{a_2} is the total linewidth of cavity mode 2. In addition, as in many theoretical or experimental articles [22–26], in Eq. (1) we do not include the magnetostrictive effect of YIG sphere because it is very weak. On the other hand, the radiation pressure effect of the microwave field on the YIG sphere is also ignored. This stems from the fact that the size of the YIG sphere is much smaller than the wavelength of microwave (e.g., the wavelength of microwave with a frequency of 10 GHz is approximately 3 cm which is much larger than the micrometer scale of YIG sphere). The experimental frequency range of cavity modes in the cavity-magnon system is on the order of GHz, due to the lack of efficient THz radiation sources and corresponding detection electronics [4].

Defining the vector of operators $\hat{\mathbf{r}} := [\hat{a}_1, \hat{a}_1^\dagger, \hat{a}_2, \hat{a}_2^\dagger, \hat{m}, \hat{m}^\dagger]^{\mathrm{T}}$, the commutation relations between the operators satisfy $[\hat{\mathbf{r}}_j, \hat{\mathbf{r}}_k] = \Xi_{jk}$, where Ξ reads as

$$\Xi := \bigoplus_{k=1}^{3} \Lambda, \quad \Lambda := \begin{bmatrix} 0 & 1 \\ -1 & 0 \end{bmatrix}. \tag{2}$$

To eliminate the time factor in Eq. (1), the rotating frame with respect to the frequency of the driving microwave ω_l is applied, and the Hamiltonian can be rewritten as

$$\begin{aligned} \hat{H}_{\mathrm{r}} = {} & \Delta_{a_1}\hat{a}_1^\dagger\hat{a}_1 + \Delta_{a_2}\hat{a}_2^\dagger\hat{a}_2 + \Delta_m\hat{m}^\dagger\hat{m} + K\hat{m}^\dagger\hat{m}\hat{m}^\dagger\hat{m} \\ & + J(\hat{a}_1^\dagger\hat{a}_2 + \hat{a}_1\hat{a}_2^\dagger) + g(\hat{a}_2^\dagger\hat{m} + \hat{a}_2\hat{m}^\dagger) \\ & + iE_l(\hat{a}_2^\dagger - \hat{a}_2), \end{aligned} \tag{3}$$

where $\Delta_i = \omega_i - \omega_l$ $(i = a_1, a_2, m)$ denotes the detuning of driving microwave from the mode i, in which $\Delta_i > 0$ and $\Delta_i < 0$ refer to red detuning and blue detuning, respectively.

B. Dynamical analysis

In addition to the driving term, also considering the environment, the cavity modes' losses and the magnon damping will also be included in dynamic evolution. Our model is thus essentially a driven-dissipative double-cavity-magnon system. To describe the dynamical behavior of the system, one can exploit the Lindblad master equation [56], i.e.,

$$\frac{d\hat{\rho}(t)}{dt} = -i[\hat{H}_{\mathrm{r}}, \hat{\rho}(t)] + \sum_{i,j=1}^{6} \frac{\Gamma_{ij}}{2}[2\hat{\mathbf{r}}_i\rho(\hat{t})\hat{\mathbf{r}}_j - \{\hat{\mathbf{r}}_j\hat{\mathbf{r}}_i, \hat{\rho}(t)\}], \tag{4}$$

where $\hat{\rho}(t)$ denotes the density matrix of the system; $\{\hat{\mathbf{r}}_i, \hat{\mathbf{r}}_j\} \in [\{\hat{a}_1, \hat{a}_1^\dagger\}, \{\hat{a}_2, \hat{a}_2^\dagger\}, \{\hat{m}, \hat{m}^\dagger\}]$ and $\{\hat{\mathbf{r}}_i, \hat{\mathbf{r}}_j\} \in [\{\hat{a}_1^\dagger, \hat{a}_1\}, \{\hat{a}_2^\dagger, \hat{a}_2\}, \{\hat{m}^\dagger, \hat{m}\}]$ represent the particle losses and the phase-insensitive linear amplification processes, respectively [56]; $\Gamma = \Gamma_{a_1} \oplus \Gamma_{a_2} \oplus \Gamma_m$ being the damping matrix, in which

$$\Gamma_{k=a_1,a_2,m} = \begin{bmatrix} 0 & \gamma_k[n(\omega_k)+1] \\ \gamma_k n(\omega_k) & 0 \end{bmatrix}, \tag{5}$$

where γ_k is the decay rate of mode k, and the Bose number $n(\omega_k) = [\exp(\omega_k/k_BT) - 1]^{-1}$ is the mean occupancy of the mode k wherein T is the environment temperature and k_B the Boltzmann constant [57,58]. Notice that for optical frequencies (about 10 THz $\sim 10^4$ THz) $n(\omega_{a_1,a_2})$ can be ignored at room temperature, however, due to the cavity modes under consideration are at microwave frequencies, so $n(\omega_{a_1,a_2})$ can be comparable to mean thermal magnon number $n(\omega_m)$ [59].

Suppose the driving microwave field is relatively strong, so each operator can be safely considered as a small quantum fluctuation above a steady-state value [57,58], i.e.,

$$\hat{\mathbf{r}} \to \langle\hat{\mathbf{r}}_{\mathbf{0}}\rangle + \delta\hat{\mathbf{r}}, \tag{6}$$

where $\langle\hat{\mathbf{r}}_{\mathbf{0}}\rangle = \mathrm{Tr}[\hat{\mathbf{r}}\hat{\rho}(\infty)]$ denoting the vector of steady-state averages and $\delta\hat{\mathbf{r}}$ is the quantum fluctuation vector around the steady-state value. According to Eq. (4), the equation of motion for the average value of an arbitrary operator $\hat{\mathcal{O}}$ is given by [56,60]

$$\frac{d\langle\hat{\mathcal{O}}\rangle}{dt} = -i\langle[\hat{\mathcal{O}}, \hat{H}_{\mathrm{r}}]\rangle + \sum_{i,j=1}^{6} \frac{\Gamma_{ij}}{2}\langle[\hat{\mathbf{r}}_j, \hat{\mathcal{O}}]\hat{\mathbf{r}}_i - \hat{\mathbf{r}}_j[\hat{\mathbf{r}}_i, \hat{\mathcal{O}}]\rangle. \tag{7}$$

Selecting $\hat{\mathcal{O}} \in \hat{\mathbf{r}}_i$ and setting $d\langle\hat{\mathcal{O}}\rangle/dt \equiv 0$ for steady state $(t \to \infty)$, one can get

$$\langle\hat{a}_1\rangle = \frac{-iJ\langle\hat{a}_2\rangle}{i\Delta_{a_1} + \gamma_{a_1}}, \tag{8}$$

$$\langle\hat{a}_2\rangle = \frac{(E_l - ig\langle\hat{m}\rangle)\left(i\Delta_{a_1} + \gamma_{a_1}\right)}{\left(i\Delta_{a_1} + \gamma_{a_1}\right)\left(i\Delta_{a_2} + \gamma_{a_2}\right) + J^2}, \tag{9}$$

$$\langle\hat{m}\rangle = \frac{-igE_l\left(i\Delta_{a_1} + \gamma_{a_1}\right)}{\mathcal{Q}\left[\left(i\Delta_{a_1} + \gamma_{a_1}\right)\left(i\Delta_{a_2} + \gamma_{a_2}\right) + J^2\right]}, \tag{10}$$

with

$$\begin{aligned} \mathcal{Q} = {} & i(\Delta_m + 2K|\langle\hat{m}\rangle|^2 + K) + \gamma_m \\ & + \frac{g^2\left(i\Delta_{a_1} + \gamma_{a_1}\right)}{\left(i\Delta_{a_1} + \gamma_{a_1}\right)\left(i\Delta_{a_2} + \gamma_{a_2}\right) + J^2}. \end{aligned} \tag{11}$$

Correspondingly, the strong driving assumption of microwave field is equivalent to the mean photon number of cavity mode 2 is large, i.e., $|\langle\hat{a}_2\rangle|^2 \gg 1$. Note that the system may exhibit multiple steady-state solutions, e.g., Eq. (10) is a unary cubic equation about the mean magnon number $|\langle\hat{m}\rangle|^2$. In this work, we only focus on parameter regimes in which the system does not exhibit multistability.

Further, applying linearization approximation (6) to (4), one can get the bilinear quantum master equation

$$\begin{aligned} \frac{d\hat{\rho}(t)}{dt} = {} & -i[\hat{H}_{\mathrm{eff}}, \hat{\rho}(t)] \\ & + \sum_{i,j=1}^{6} \frac{\Gamma_{ij}}{2}[2\delta\hat{\mathbf{r}}_i\rho(\hat{t})\delta\hat{\mathbf{r}}_j - \{\delta\hat{\mathbf{r}}_j\delta\hat{\mathbf{r}}_i, \hat{\rho}(t)\}] \end{aligned} \tag{12}$$

with linearized effective Hamiltonian

$$\begin{aligned} \hat{H}_{\mathrm{eff}} = {} & \Delta_1\delta\hat{a}_1^\dagger\delta\hat{a}_1 + \Delta_2\delta\hat{a}_2^\dagger\delta\hat{a}_2 + \Delta_{\mathrm{eff}}\delta\hat{m}^\dagger\delta\hat{m} \\ & + K[\langle\hat{m}\rangle^2\delta\hat{m}^\dagger\delta\hat{m}^\dagger + \langle\hat{m}\rangle^{*2}\delta\hat{m}\delta\hat{m}] \\ & + J(\delta\hat{a}_1^\dagger\delta\hat{a}_2 + \delta\hat{a}_1\delta\hat{a}_2^\dagger) + g(\delta\hat{a}_2^\dagger\delta\hat{m} + \delta\hat{a}_2\delta\hat{m}^\dagger), \end{aligned} \tag{13}$$

where only the quadratic order terms of fluctuations are retained and $\Delta_{\mathrm{eff}} = \Delta_m + 4K|\langle\hat{m}\rangle|^2$ is the effective detuning of magnon in the presence of the Kerr effect.

In particular, this work strongly relies on the framework of Gaussian state, wherein it is convenient to model our system

by dimensionless quadrature operators in the phase space. Defining Hermitian quadrature operators [57,58]

$$\hat{Q}_o := (\hat{o} + \hat{o}^\dagger)/\sqrt{2}, \tag{14}$$

$$\hat{P}_o := (\hat{o} - \hat{o}^\dagger)/\sqrt{2}i, \tag{15}$$

where $o = a_1, a_2$, and m; the corresponding fluctuations are $\delta\hat{Q}_o$ and $\delta\hat{P}_o$. The Lyapunov equation for the steady-state covariance matrix $\mathcal{V}$ can be obtained through Eq. (12), i.e.,

$$\mathfrak{A}\mathcal{V} + \mathcal{V}\mathfrak{A}^{\mathrm{T}} = -\mathfrak{D}, \tag{16}$$

with

$$\mathfrak{A} = \begin{bmatrix} -\gamma_{a_1} & \Delta_{a_1} & 0 & J & 0 & 0 \\ -\Delta_{a_1} & -\gamma_{a_1} & -J & 0 & 0 & 0 \\ 0 & J & -\gamma_{a_2} & \Delta_{a_2} & 0 & g \\ -J & 0 & -\Delta_{a_2} & -\gamma_{a_2} & -g & 0 \\ 0 & 0 & 0 & g & \Re_+ & \Im_+ \\ 0 & 0 & -g & 0 & \Im_- & \Re_- \end{bmatrix} \tag{17}$$

and

$$\begin{aligned} \mathfrak{D} = \mathrm{diag}\big\{&\big[2n\big(\omega_{a_1}\big)+1\big]\gamma_{a_1}, \big[2n\big(\omega_{a_1}\big)+1\big]\gamma_{a_1}, \\ &\big[2n\big(\omega_{a_2}\big)+1\big]\gamma_{a_2}, \big[2n\big(\omega_{a_2}\big)+1\big]\gamma_{a_2}, \\ &[2n(\omega_m)+1]\gamma_m, [2n(\omega_m)+1]\gamma_m\big\}, \end{aligned} \tag{18}$$

where $\mathfrak{A}$ and $\mathfrak{D}$ are the drift and diffusion matrices, respectively; $\Re_\pm = -\gamma_m \pm 2\,\mathrm{Im}(\langle\hat{m}\rangle^2)K$ and $\Im_\pm = \pm(\Delta_{\mathrm{eff}} + K) - 2\,\mathrm{Re}(\langle\hat{m}\rangle^2)K$.

The covariance matrix $\mathcal{V}$'s ij element are given by $\mathcal{V}_{ij} := \langle\delta\hat{\mathbf{R}}_i(\infty)\delta\hat{\mathbf{R}}_j(\infty) + \delta\hat{\mathbf{R}}_j(\infty)\delta\hat{\mathbf{R}}_i(\infty)\rangle/2$, where fluctuation quadrature operator vector $\delta\hat{\mathbf{R}} := [\delta\hat{Q}_{a_1}, \delta\hat{P}_{a_1}, \delta\hat{Q}_{a_2}, \delta\hat{P}_{a_2}, \delta\hat{Q}_m, \delta\hat{P}_m]^{\mathrm{T}}$ is defined and satisfies commutation relations $[\delta\hat{\mathbf{R}}_j, \delta\hat{\mathbf{R}}_k] = i\Xi_{jk}$. This indicates that the steady second moment of the system is encoded on the covariance matrix $\mathcal{V}$, formally

$$\mathcal{V} := \begin{bmatrix} L_{a_1} & C_{a_1,a_2} & C_{a_1,m} \\ C^{\mathrm{T}}_{a_2,a_1} & L_{a_2} & C_{a_2,m} \\ C^{\mathrm{T}}_{m,a_1} & C^{\mathrm{T}}_{m,a_2} & L_m \end{bmatrix}, \tag{19}$$

where L_i and $C_{i,j}$ being a 2×2 subblock matrices of $\mathcal{V}$ ($i, j = a_1, a_2, m$), they represent the local properties of mode i and the quantum correlation between modes i and j, respectively. Here, we emphasize that our current work requires the cavity-magnon system to be in the stable region. We have selected proper parameters to satisfy the specific stability condition shown in Appendix B.

III. ESTIMATION OF PHOTON-MAGNON COUPLING STRENGTH

With QFI, the precision limit of estimating the P-M coupling strength g is quantified by the quantum Cramér-Rao bound (QCRB) inequality, i.e. [28–30],

$$\mathrm{Var}(\hat{g}) \geqslant \frac{1}{\mathcal{N}\mathcal{F}_g}, \tag{20}$$

where $\mathrm{Var}(\hat{g})$ is the mean-square error of unbiased estimator; $\mathcal{N}$ is the number of independent repetition of the estimation protocol. In practical experiments, it is more feasible to measure only one of the subsystems. The interaction between subsystems leads to the transfer of interested parameter information between them. Thus, two questions naturally arise: (1) What is the precision limit for estimating g based on each subsystem? (2) Which is the optimal subsystem for estimating g (defined as the subsystem that contains the most information about g under the same conditions)?

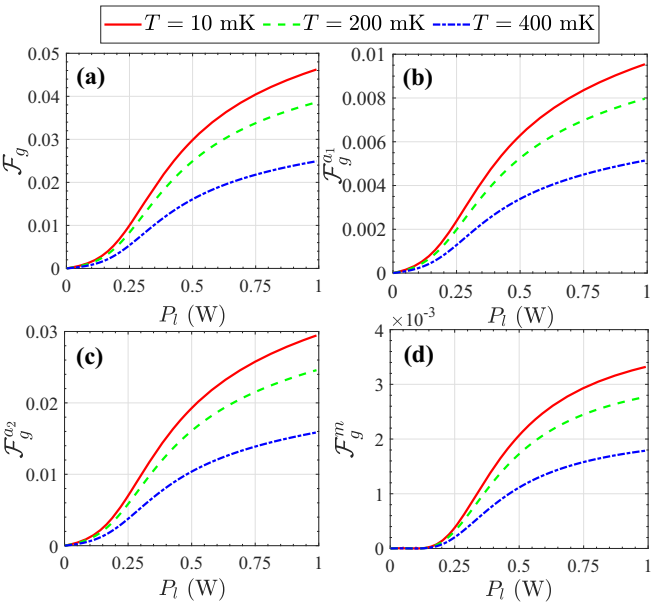

FIG. 2. The QFIs versus the microwave driving power at different environment temperatures T, where QFI for (a) the global system, (b) the cavity mode 1, (c) the cavity mode 2, (d) the magnon mode.

In this section, we explore how various physical factors affect the estimation precision of the P-M coupling rate, such as the driving power P_l, the environment temperature T, the dissipation rates of cavity modes and magnon mode, the Kerr coefficient K, the photon tunneling rate J, the cavity modes detuning Δ_a, and the magnon detuning Δ_m. We then explore the optimal subsystem for estimating the P-M coupling parameter. Finally, the performance of Gaussian measurements performed on the optimal subsystem is evaluated. Particularly, in what follows, we obtain QFI mainly through numerical simulations, as the analytical solution is too cumbersome. Details of the Gaussian parameter estimation in this hybrid system are provided in Appendix C. For simplicity, we assume that the parameters of the two cavities are completely consistent. Unless stated otherwise, here and in what follows, the parameters are chosen as $P_l = 500$ mW, $\omega_l = 2\pi \times 10$ GHz, $T = 10$ mK, $\gamma_{a_1} = \gamma_{a_2} = \gamma_a = 2\pi \times 5$ MHz, $\gamma_m = 2\pi \times 40$ MHz, $\Delta_{a_1} = \Delta_{a_2} = \Delta_a = 2\pi \times 40$ MHz, $\Delta_m = 2\pi \times 60$ MHz, $K = 2\pi \times 2\ \mu$Hz, $J = 2\pi \times 26$ MHz, $g = 2\pi \times 41$ MHz, whose values are mostly based on the latest experimental data [4–6,12,20,22].

A. Effect of power and temperature

As shown in Fig. 2, the QFIs for the whole system and the three subsystems are plotted as a function of microwave

driving power P_l at different environment temperatures, manifesting that all QFIs are nearly zero when the driving is weak ($P_l = 1$ mW), i.e., the error for estimating the P-M coupling parameter is relatively large. However, all QFIs are gradually enhanced with the increase of P_l, implying that microwave driving is beneficial for improving the estimation precision of g. This is easy to understand. Since the increase of external driving directly gives rise to an increase in the mean particle number of various modes in the double-cavity-magnon system, and the effective magnetic-dipole interaction is also enhanced, resulting in a reduced estimation error. Here, we emphasize that the mean particle number of all modes is much greater than 1 even when $P_l = 1$ mW, which ensures the linearization approximation holds. In addition, in the case of $P_l = 1$ W, the mean magnon number $\langle \hat{m}^\dagger \hat{m} \rangle \simeq 6 \times 10^{13} \ll 2S = 1.75 \times 10^{17}$ holds for a 250-μm-diameter YIG sphere, indicating that the low-lying excitations assumption required for utilizing Holstein-Primakoff transformation in deriving the Hamiltonian $\hat{H}$ has not been violated (see Appendix A).

Furthermore, one can see that the P-M coupling's information contained in the global state is always greater than that in the state of each subsystem. This also indirectly reflects the non-negative property of QFI, i.e., the more subsystems used, the higher QFI obtained. On the other hand, the QFI of the global system is always greater than or equal to the independent summation of that of each subsystem. This is because the global system has some additional quantum correlation terms [see $C_{i,j}$ in Eq. (19)] compared to the direct sum of the subsystems, where the quantum correlation terms also contain information about g. Particularly, the imprint of g is mainly in cavity mode 2, followed by cavity mode 1, while the magnon mode contains the least, i.e., $\mathcal{F}_g^{a_2} > \mathcal{F}_g^{a_1} > \mathcal{F}_g^{m}$ in the given parameter regime. Obviously, at this point the cavity mode 2 is the optimal subsystem for estimating g. Physically, the distribution of the imprint of g among subsystems relies on the interactions and correlations between subsystems. Later, we will specifically discuss this issue.

Consistent with our expectation, as the temperature increases (red → green → blue), all the QFIs drop off, indicating that adding thermal fluctuation to the system always decreases the estimation precision. Physically, the thermal fluctuations in general lead to a degradation of the quantum correlations of the system, thereby increasing the estimation error of P-M coupling rate. Note that the boosting effects of the quantum resources on estimation precision have been realized by many researchers working in the field.

B. Effect of the damping channels

It is of practical importance to investigate the influence of the dissipation rate on the estimation error. Presented in Fig. 3, the density plot represents the global QFI $\mathcal{F}_g$ as a function of the cavity mode decay rate γ_a and the magnon damping γ_m. According to Fig. 3, it reveals that with the increase of γ_m keeping γ_a unaltered $\mathcal{F}_g$ monotonically decreases, i.e., the magnon dissipation is always detrimental for estimating the P-M coupling rate. In contrast, for a fixed γ_m the estimation error first decreases and then increases with the increase of cavity decay rate γ_a. This indicates that there exists an optimized value of γ_a where the estimation error reaches a minimum.

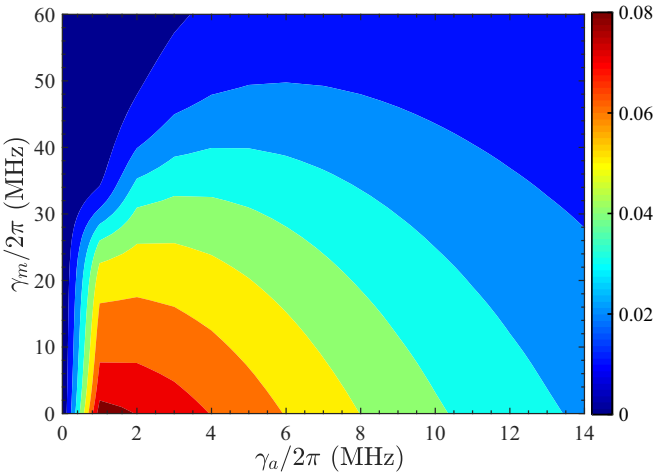

FIG. 3. The density plot represents the QFI for the global system as a function of cavity mode loss γ_a and magnon damping γ_m.

The physical reason behind this counterintuitive phenomenon is that when $\sqrt{\gamma_a}$ is small, increasing γ_a causes the increase of the microwave driving strength owing to $E_l \propto \sqrt{\gamma_a}$, resulting in enhancement of estimation precision (using the results of Fig. 2). Nevertheless, when γ_a increases further, the dissipation of the cavity modes dominates the dynamics, which yields a significant increase in the estimation error. As a result, the final estimation precision is determined by the competition between the two opposite effects caused by the cavity mode loss. The behavior of the QFI of each subsystem is rather similar to that of the global system, hence, their figures are omitted here.

In addition, we should also point out that if the loss rates of the two microwave cavities are different, when fixing the rate of cavity mode 1, increasing that of cavity mode 2 will obtain similar results. However, keeping the loss rate of cavity mode 2 fixed while increasing that of cavity mode 1 only leads to a decrease in estimation precision. This is due to the fact the driving field is applied on the cavity mode 2 rather than the cavity mode 1.

C. Effect of Kerr nonlinearity and photon tunneling

In Fig. 4, the density plot denotes the QFIs as a function of the Kerr coefficient K and the photon tunneling rate J, manifesting that although the magnon mode is a necessary element to realize P-M coupling, most of the global QFI comes mainly from the contribution of the two cavity mode subsystems, with a small contribution from the magnon. One reason is that the damping of the magnon is greater than that of the cavity modes (the incoherence effect of the magnon modes is greater), while another reason is the photon-tunneling-induced cavity modes swap, i.e., dissemination of information about g. In this sense, cavity mode 1 can act as an auxiliary mode to carry information about the P-M coupling rate, which may help improve estimation precision. Indeed, we can see that by appropriately designing the tunneling rate J, the global QFI increases, manifesting that the auxiliary cavity can reduce the estimation error in comparison with the unassisted case ($J = 0$). This is because effective P-M coupling depends not

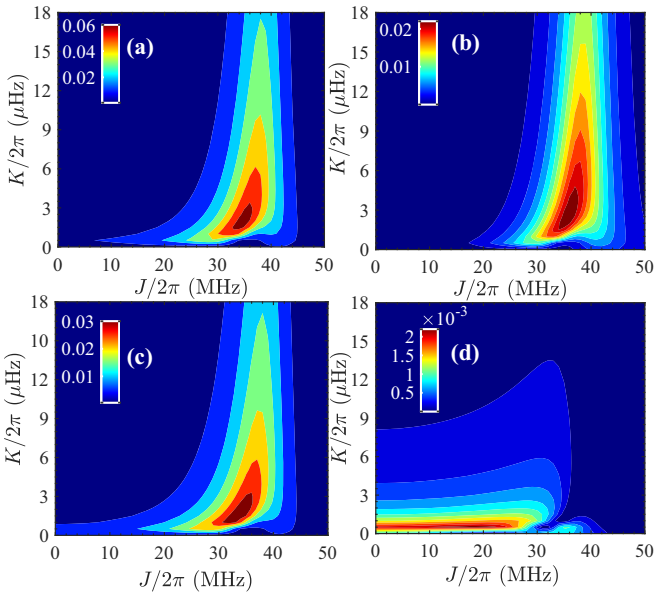

FIG. 4. The QFIs vary with the Kerr coefficient K and the photon-tunneling rate J, where QFI for (a) the global system, (b) the cavity mode 1, (c) the cavity mode 2, (d) the magnon mode.

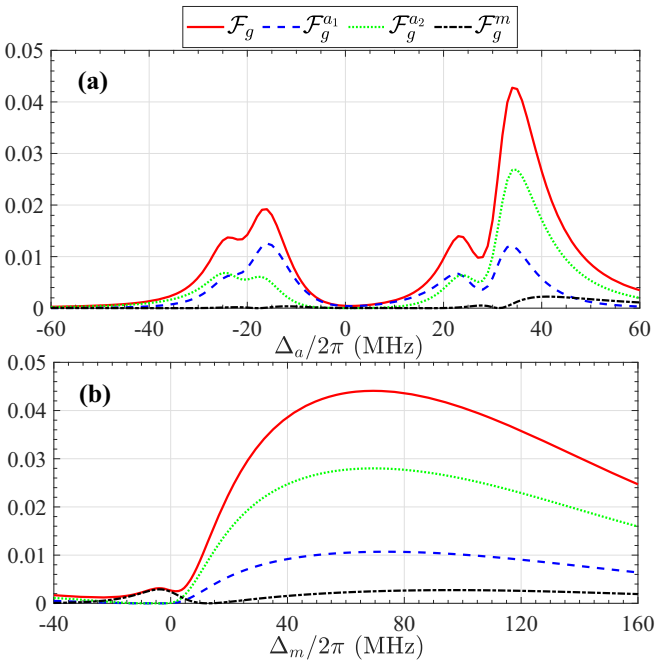

FIG. 5. The QFIs of global system and subsystems as a function of (a) the cavity mode detuning Δ_a and (b) the magnon detuning Δ_m, respectively.

only on the coupling strength, but is also closely related to the frequency matching between the modes, and photon-tunneling interactions can adjust the frequencies of the mixed cavity modes. Similar to the global QFI, the QFI of cavity mode 2 is also significantly improved under appropriate photon tunneling rates. This is of great practical importance because, as we will see later, the cavity mode 2 is the optimal subsystem for making Gaussian measurements in most parameter regions. Note that when the photon-tunneling interaction is completely dominant (i.e., J is sufficiently large), this is also detrimental to the estimation since the magnetic-dipole interaction can be almost neglected in the cavity-magnon system.

On the other hand, all QFIs display a tendency to increase first and then decrease when fixed J increases K. We can see that the appropriate Kerr coefficient can also greatly enhance the estimation precision compared to the case without the Kerr effect. Physically, this is due to the fact that the Kerr nonlinear effect causes quantum squeezing on the magnon. In addition, the appropriate Kerr-effect-induced magnon frequency shift is also a reason for the improved estimation precision, as it can enhance effective P-M coupling. Nevertheless, as K is further increased, the effective frequency difference between the magnon and the cavity modes is increased. This will weaken the effective P-M coupling interaction, increasing estimation error. The above analysis indicates that, when other parameters are fixed, a wise match between the Kerr nonlinearity coefficient and the photon-tunneling rate is required to obtain the highest estimation precision.

D. Effect of detuning

In Fig. 5(a), we depict the QFIs as a function of the cavity mode detuning Δ_a, showing that the global QFI still mainly comes from the two cavity modes. In particular, we can see that there are two peaks (one is the main peak and the other is the secondary peak) on each of the red, green, and blue curves in the red-detuned region. Similar results are also observed in the blue-detuned region, but the secondary peak is not significant. Physically, these valley-peak structures of QFIs originate from the presence of two hybridized cavity modes interacting with the magnon mode. Particularly, the locations of these peaks are not only dependent on the selection of Δ_m but are also closely related to photon tunneling and the Kerr effect since both can adjust the effective mode detuning. The normal mode picture in Appendix D makes this clear. In addition, we find that the red-detuned region is more conducive to estimating g, giving the highest estimation precision. This indicates that even including photon tunneling and Kerr nonlinear effects, in the red-detuning region, the effective P-M coupling is still relatively strong due to Δ_m being greater than 0. Note that this result holds without considering tunneling and Kerr nonlinearity effects. This is because the P-M coupling is essentially beam-splitter-like coupling, and the closer the frequencies of the two modes are, the stronger the coupling will be.

Figure 5(b) plots the QFIs as a function of the magnon detuning Δ_m. One can see that in the $\Delta_m < 0$ region, all QFIs are relatively small, implying a higher estimation error. In the $\Delta_m > 0$ region, all QFI curves exhibit a wide peak, indicating that we are easier to obtain high estimation precision. This is because the Kerr effect can induce an appreciable frequency shift of the magnon mode, resulting in a wide peak that is insensitive to Δ_m [25]. Note that the frequency of the magnon can be flexibly adjusted by the external bias magnetic field H_B, which indirectly changes the Δ_m, thus realizing the modulation of the estimation precision. This means that when other parameters are fixed, there exists some ideal H_B that can provide relatively high estimation precision.

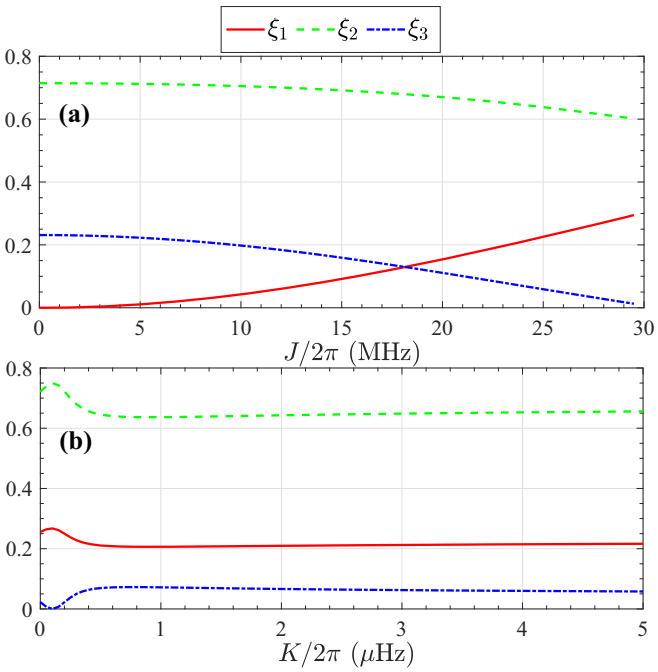

FIG. 6. The ratio of the QFI of the subsystem to that of the global system is shown as a function of (a) the photon-tunneling rate J and (b) the Kerr coefficient K, respectively.

E. Optimal subsystem for estimating g

Notice that it is very difficult or even infeasible to measure the entire double-cavity-magnon system owing to the limitations of the measurement means. Thus, a wise choice would be to access and measure one of the subsystems. In this scenario, it becomes crucial to determine the optimal subsystem, i.e., the one that contains the most information about the estimated parameter. To this end, we define the ratio of the QFI of each subsystem to the global QFI, namely, $\xi_1 = \mathcal{F}_g^{a_1}/\mathcal{F}_g$, $\xi_2 = \mathcal{F}_g^{a_2}/\mathcal{F}_g$, and $\xi_3 = \mathcal{F}_g^{m}/\mathcal{F}_g$, respectively.

In the discussion about Fig. 2, we have pointed out that cavity mode 2 is the optimal subsystem for estimating the P-M coupling strength, indicating that ξ_2 is greater than ξ_1 and ξ_3. In addition, when studying the impact of damping channels on estimation precision, the result that cavity mode 2 is the optimal subsystem still holds (note that in order to avoid figure duplication, the QFIs of the subsystems are not drawn in Fig. 3). However, according to Fig. 5, we find that cavity mode 2 is not always the optimal subsystem, as seen in the blue-detuned region. But in the red-detuned region, the cavity mode 2 is an ideal candidate for extracting information from g. Below, we will focus on the impact of photon-tunneling rate J and Kerr nonlinearity coefficient K on ξ_j $(j = 1, 2, 3)$.

Figure 6(a) plots ξ_j $(j = 1, 2, 3)$ as functions of the photon-tunneling strength J, indicating that when $J = 0, \xi_2 > \xi_3 > \xi_1 = 0$ holds. In other words, accessing cavity mode 2 is able to pick up the most information about the P-M coupling parameter, followed by the magnon, while cavity mode 1 does not contain information about g. This originates from the fact that no information can swap between cavity modes 1 and 2 without photon hopping interaction, so that $\xi_1 = 0$. The reason for $\xi_2 > \xi_3$ is that the photon number of the cavity mode 2 is more than the magnon number owing to the direct driving and $\gamma_a < \gamma_m$. With the increase of J, one finds that ξ_2 and ξ_3 decrease simultaneously, while ξ_1 increases. This reveals that part of the information about g is transferred to cavity mode 1 via the photon-tunneling interaction. Moreover, the stronger the photon-tunneling effect, the greater the information containing g in cavity mode 1, resulting in $\xi_2 > \xi_1 > \xi_3$. In particular, $\xi_2 > \xi_1, \xi_3$ holds all the time, manifesting that the amount of information about the P-M coupling rate in cavity mode 2 is always the most, i.e., the cavity mode 2 is the optimal subsystem for estimating g for the given parameter regime.

In Fig. 6(b), we present behaviors of ξ_j $(j = 1, 2, 3)$ versus the Kerr coefficient K. One can see that when K starts increasing from 0, ξ_1 and ξ_2 increase first and then decrease, while ξ_3 has the opposite trend. This is due to the fact that the tradeoff and competition between the P-M coupling and the photon tunneling can be affected by the Kerr self-interaction of magnon, while the first two play a decisive role in the exchange of information between subsystems. With a further increase in K, the self-interaction of magnon completely surpasses photon tunneling and P-M coupling, so that the distribution of information in each subsystem no longer changes significantly. Indeed, when changing J or K, the behavior of ξ_3 is always opposite to that of the other two, which reflects information swap very well. Importantly, $\xi_2 > \xi_1, \xi_3$ holds all the time, i.e., the cavity mode 2 is always the optimal subsystem for estimating the P-M coupling rate.

F. Performance analysis of Gaussian measurements

According to Sec. III E, we already know that cavity mode 2 is the optimal subsystem for estimating g in most parameter regions except in the blue-detuned region where the QFI is small. This means that accessing cavity mode 2 for obtaining information about the P-M coupling parameter is relatively high efficiency in most cases. Consequently, considering that only one subsystem can be accessed, we only focus on the case of the information about g obtained by performing measurements on the cavity mode 2. We will explore which Gaussian detection method can achieve higher precision for estimating g by comparing the CFIs of heterodyne detection ($F_{g,\mathrm{He}}^{a_2}$), homodyne detection ($F_{g,\mathrm{Ho}}^{\hat{Q}_{a_2}}$ and $F_{g,\mathrm{Ho}}^{\hat{P}_{a_2}}$), and the optimal Gaussian measurement (F_g^{OGM}). Note that the details for calculating the CFIs of these measurement settings are provided in Appendix C 2.

In Fig. 7, we compare the ultimate precision bound given by QFI $\mathcal{F}_g^{a_2}$ with the precisions achieved through the Gaussian measurements. One finds that $\mathcal{F}_g^{a_2} > F_{g,\mathrm{Ho}}^{\hat{Q}_{a_2}} > F_{g,\mathrm{He}}^{a_2} > F_{g,\mathrm{Ho}}^{\hat{P}_{a_2}}$ always holds, indicating that neither widely available homodyne detection nor heterodyne detection is the optimal measurement setup. In addition, the homodyne measurement for amplitude quadrature $\hat{Q}_{a_2}$ is better than the heterodyne detection, and the worst scheme is the homodyne detection for phase quadrature $\hat{P}_{a_2}$. Roughly speaking, measuring the $\hat{P}_{a_2}$ quadrature is hardly helpful for estimating the P-M coupling because the obtained CFI is too small. Physically, this is because the P-M coupling mainly affects the amplitude of cavity mode 2 (i.e., mean photon number of cavity mode 2)

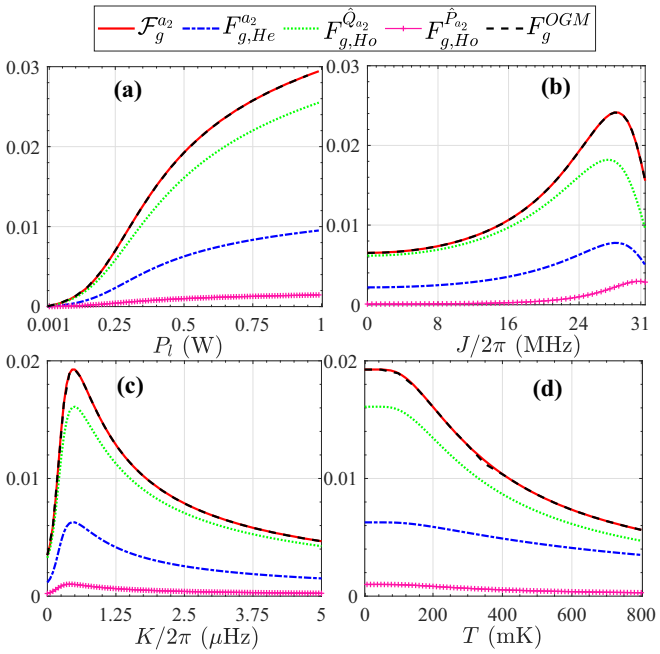

FIG. 7. The QFI $\mathcal{F}_g^{a_2}$ and CFIs for the cavity mode 2 against (a) the microwave driving power P_l, (b) the photon tunneling strength J, (c) the Kerr coefficient K, (d) the ambient temperature T, where $F_{g,\mathrm{He}}^{a_2}$, $F_{g,\mathrm{Ho}}^{\hat{Q}_{a_2}}$, $F_{g,\mathrm{Ho}}^{\hat{P}_{a_2}}$, and F_g^{OGM} corresponding to heterodyne detection, homodyne detection for $\hat{Q}_{a_2}$ and $\hat{P}_{a_2}$ quadrature operators, and optimal Gaussian measurement, respectively.

rather than the phase, so the amplitude quadrature of cavity mode 2 contains more information about g. In particular, we also obtain the CFIs corresponding to the optimal Gaussian measurement by means of semidefinite programming (see black dashed lines). We find that the red solid line and the black dashed line almost overlap in all subfigures, i.e., the optimal Gaussian measurement almost constitutes the optimal setup for estimating the P-M coupling strength.

It should be pointed out that the optimal positive-operator-valued measurement setup is constituted by a set of projection operators over the eigenvectors of symmetric logarithmic derivative $L_g^{a_2}$, where $L_g^{a_2}$ is composed of the first moments and covariance matrix of the cavity mode 2 [61–64]. In principle, one can always theoretically construct optimal measurements based on this conclusion. However, such optimal measurement is generally not experimentally feasible, especially in the current model where such interactions are relatively complex. In this scenario, the optimal Gaussian measurement is much more favored because it is experimentally feasible. In addition, the practical imperfections tend to offset the difference between optimal and nearly optimal setups in the laboratory [65]. This also reflects the fact that the estimation precision limit given by $\mathcal{F}_g^{a_2}$ is experimentally achievable. Unfortunately, due to difficulties in mathematical techniques, we do not yet know the specific form of the optimal Gaussian measurement. In theory, it should be the product of the quadrature operators of the observed mode (e.g., complex combination of amplitude and phase quadrature operators). In addition, it may depend on the values of the parameters to be evaluated. In this sense, this optimal Gaussian measurement needs to be implemented adaptively by accumulated data. We will further investigate such a question elsewhere, which has enormous practical significance.

IV. CONCLUSION AND DISCUSSION

In summary, we have explored the quantum parameter estimation problem of the P-M coupling strength in a driven-dissipative double-cavity-magnon system, where one cavity is primary and the other is auxiliary. We found that (i) with the increase of the driving power, the estimation error gradually decreases; (ii) temperature and magnon damping are always detrimental for estimating the P-M coupling strength; (iii) the dissipation rate of the cavity mode does not always have a detrimental effect on the estimation error, and the existence of a critical dissipation rate giving the highest estimation precision; (iv) by designing appropriate Kerr coefficient and photon tunneling rate, the estimation error can be significantly reduced; (v) compared to the blue-detuned region, the red-detuned region of the cavities is more conducive to achieving high-precision estimation; moreover, the external bias magnetic field applied to the YIG sphere can indirectly adjust estimation error due to its ability to modulate magnon detuning; (vi) the summation of QFI for all subsystems is always less than or equal to the QFI of the global system. Our analysis also revealed that the optimal subsystem for carrying out measurements and estimations is the primary cavity mode since in most parameter regions the majority of information about the P-M coupling rate is encoded in its reduced state.

Further, we explored the CFI obtained by performing different Gaussian measurements on the primary cavity mode and compared them with QFI to evaluate the practical performance of measurements. The results indicated that homodyne and heterodyne detections are not optimal measurement strategies for the extraction of the P-M coupling information. The homodyne detection for amplitude quadrature surpasses the heterodyne detection, and the worst is the homodyne detection for phase quadrature. Particularly, the optimal Gaussian measurement is almost the optimal measurement strategy, i.e., it can extract almost all the information about the P-M coupling parameter from the primary cavity mode. We note that increasing the number of auxiliary cavities can improve the QFI, but at the same time introduces more dissipations and makes the experiment more difficult. We also note that once the P-M coupling strength is comparable to the magnon or cavity mode frequencies, one can no longer consider photon and magnon dissipation separately, as is done here. Potentially, we can also investigate the estimation problem of other parameters in cavity-magnon systems, such as photon-tunneling rate, frequency, and Kerr coefficient of magnons. However, the optimal structure of the composite system may not be a double-cavity structure with one primary and one auxiliary. We believe that this work provides some insights into the use of magnetic-dipole interaction for quantum precision measurements or quantum information processing.

Finally, we should point out that our approach is based on the linearization approximation of the cavity optomechanics and cavity magnomechanics [57,58], and the QFI is embedded in the steady-state values and quantum fluctuations of the cavity-magnon system. However, when the cavity-magnon

system is not in a steady state, e.g., when the system dynamics exhibits limit cycles or chaos, the linearization approximation fails and the Gaussian state no longer effectively describes the quantum properties of the system, the strict quantum master equations should be used instead to analyze the QFI. In this case, the system may be able to provide a larger QFI in comparison with our current results. There have been reports that chaotic dynamics can assist quantum parameter estimation in some parameter regions [66], but its physical realization is challenging.

Besides, more recently, the experimental extraction of the QFI has received widespread attention and made some important progress [67–70]. These studies are mainly based on spin systems and nitrogen-vacancy (NV) centers. It should be emphasized that QFI itself does not directly correspond to observable Hermitian operators, but it is closely related to many measurable physical quantities, such as asymmetric cross-correlation spectrum [29], energy fluctuation [68], and quantum geometric tensor [70]. This is the principle of extracting QFI in experiments. However, to the best of our knowledge, the experimental extraction of QFI in continuous variable systems has not been reported until now. It is worth mentioning that the first moment and covariance matrix of Gaussian steady state in cavity-magnon systems can be reconstructed in the laboratory [4–7], and the relevant technology of Gaussian measurement is relatively mature. Our theory is therefore expected to be experimentally confirmed. Nevertheless, if the cavity-magnon system is not in a steady state, its quantum characteristics cannot be represented by using the first moment and covariance matrix. It is thus necessary to capture quantum states at different times through quantum state tomography technology, which is a great challenge for experiments due to the system being infinitely dimensional.

ACKNOWLEDGMENTS

This work was supported by the Innovation Program for Quantum Science and Technology (Grant No. 2021ZD0303200); the National Key Research and Development Program of China (Grant No. 2016YFA0302001); the National Science Foundation of China (Grants No. 12374328, No. 11974116, No. 12234014, and No. 11654005); the Shanghai Municipal Science and Technology Major Project (Grant No. 2019SHZDZX01); the Fundamental Research Funds for the Central Universities; the Chinese National Youth Talent Support Program, and the Shanghai talent program.

APPENDIX A: DERIVATION OF HAMILTONIAN FOR YIG SPHERE AND CAVITY MODE 2

The quantized interaction form between cavity modes (coupled cavity) is well known to everyone [57]. We thus will only provide a detailed introduction to the interaction between the YIG sphere and cavity mode 2. The cavity mode 2 includes electric field energy and magnetic field energy, while the magnetized YIG sphere includes Zeeman energy, demagnetization energy, and anisotropic energy of magnetocrystalline, and there is magnetic-dipole interaction between the two. Therefore, the total Hamiltonian can be written as [5,6,71]

$$\hat{H}_{\mathrm{a_2m}} = \frac{1}{2}\int\left(\varepsilon_0\mathbf{E}^2 + \frac{\mathbf{B}^2}{\mu_0}\right)d\mathbf{v} - \int \mathbf{M}\cdot\mathbf{H}_B d\mathbf{v} - \frac{\mu_0}{2}\int \mathbf{M}\cdot\mathbf{H}_{\mathrm{an}} d\mathbf{v} - \mu_0\int \mathbf{M}\cdot\mathbf{B}\, d\mathbf{v}, \tag{A1}$$

where $\mathbf{E}$ and $\mathbf{B}$ are the electric and magnetic components of the electromagnetic field inside the cavity 2, respectively; ε_0 and μ_0 are, respectively, the vacuum permittivity and vacuum permeability; $\mathbf{H}_B = H_B\vec{\mathbf{e}}_{\mathrm{z}}$ being the stable magnetic field applied along the Z axis on the YIG sphere, aimed at magnetizing the YIG sphere. The corresponding magnetization strength is $\mathbf{M} = \gamma_e\,\mathbf{S}/V_m = (\mathrm{M_x}, \mathrm{M_y}, \mathrm{M_z})$, in which $\mathbf{S} \equiv (S_{\mathrm{x}}, S_{\mathrm{y}}, S_{\mathrm{z}})$ denotes the macrospin and V_m the volume of the YIG sphere; $\mathbf{H}_{\mathrm{an}} = (-2K_{\mathrm{an}}\mathrm{M_z}/\mathrm{M}_b^2)\vec{\mathbf{e}}_{\mathrm{z}}$ represents the anisotropic field owing to the magnetocrystalline anisotropy (relying on the angle between the crystallographic axis of the YIG sphere and the direction of the externally applied stable magnetic field) [72], in which K_{an} and M_b are the first-order anisotropy constant of the YIG sphere and the saturation magnetization, respectively; the last term represents the magnetic-dipole interaction between cavity mode 2 and magnon. Note that demagnetization energy is ignored in Eq. (A1) because it is a constant term [5,6].

Suppose that the magnetic field direction inside the cavity 2 is along the X axis, i.e., $\mathbf{B} = -\sqrt{\omega_{a_2}/\mu_0 V_a}(\hat{a}_2 + \hat{a}_2^\dagger)\vec{\mathbf{e}}_{\mathrm{x}}$, where V_a is the volume of the cavity 2. One can introduce magnon mode to represent a collective excitation of a large number of spins by the Holstein-Primakoff transform [73]

$$\hat{S}_z = S - \hat{m}^\dagger\hat{m}, \tag{A2a}$$

$$\hat{S}_+ = \sqrt{2S - \hat{m}^\dagger\hat{m}}\,\hat{m}, \tag{A2b}$$

$$\hat{S}_- = \hat{m}^\dagger\sqrt{2S - \hat{m}^\dagger\hat{m}}, \tag{A2c}$$

$$\hat{S}_\pm = \hat{S}_x \pm i\hat{S}_y, \tag{A2d}$$

where S is the total spin number of the YIG sphere. In particular, $2S \gg \langle\hat{m}^\dagger\hat{m}\rangle$ in general holds owing to a fact $2S = 5\rho V_m$ is very huge for a YIG sphere with spin density $\rho \approx 4.22 \times 10^{27}\ \mathrm{m}^{-3}$ [4–6]. This results in the following being approximately valid: $\hat{S}_+ \simeq \sqrt{2S}\hat{m}$ and $\hat{S}_- \simeq \sqrt{2S}\hat{m}^\dagger$. By putting the pieces together, the $\hat{H}_{\mathrm{a_2m}}$ can be rewritten as

$$\hat{H}_{\mathrm{a_2m}} = \omega_{a_2}\hat{a}_2^\dagger\hat{a}_2 - \gamma_e H_B\hat{S}_z + \frac{\mu_0 K_{\mathrm{an}}\gamma_e^2\hat{S}_z^2}{V_m\mathrm{M}_b^2} + g_{am}(\hat{a}_2 + \hat{a}_2^\dagger)(\hat{S}_+ + \hat{S}_-), \tag{A3}$$

where $g_{am} = \sqrt{\mu_0\gamma_e^2\omega_{a_2}/4V_a}$ is the coupling strength between the cavity mode 2 and the spins. Using $\sqrt{2S}\hat{m}$ and $\sqrt{2S}\hat{m}^\dagger$ to replace $\hat{S}_\pm$, and considering the rotating-wave approximation, one can finally obtain

$$\hat{H}_{\mathrm{a_2m}} = \omega_{a_2}\hat{a}_2^\dagger\hat{a}_2 + \omega_m\hat{m}^\dagger\hat{m} + K\hat{m}^\dagger\hat{m}\hat{m}^\dagger\hat{m} + g(\hat{a}_2\hat{m}^\dagger + \hat{a}_2^\dagger\hat{m}), \tag{A4}$$

where $\omega_m = \gamma_e H_B - 2\mu_0 K_{\mathrm{an}}\gamma_e^2 S/V_m\mathrm{M}_b^2$ being the frequency of the magnon, indicating that the frequency of the magnon can be tuned by the bias magnetic field; $K = \mu_0 K_{\mathrm{an}}\gamma_e^2/V_m\mathrm{M}_b^2$ is Kerr nonlinear coefficient; $g = \sqrt{2S}g_{am}$ stands for the P-M coupling strength.

APPENDIX B: STABILITY CONDITIONS FOR THE SYSTEM

The stability of the system is ensured by Routh-Hurwitz criterion [74], namely, the all eigenvalues of the drift matrix $\mathfrak{A}$ have negative real parts, indicating that the system is stable. To this end, we need to evaluate the characteristic equation of $\mathfrak{A}$, i.e., $|\mathfrak{A} - \lambda \mathbb{1}_6| = 0$, yielding the characteristic equation

$$\lambda^6 + \alpha_1\lambda^5 + \alpha_2\lambda^4 + \alpha_3\lambda^3 + \alpha_4\lambda^2 + \alpha_5\lambda + \alpha_6 = 0, \quad \text{(B1)}$$

where

$$\alpha_0 = 1, \quad \text{(B2)}$$
$$\alpha_1 = 4\gamma_a - \eta_1, \quad \text{(B3)}$$
$$\alpha_2 = 2(g^2 + J^2) + 6\gamma_a^2 + 2\Delta_a^2 - 4\eta_1 + \eta_2, \quad \text{(B4)}$$
$$\alpha_3 = 4\gamma_a^3 - \eta_1(g^2 + 2\eta_5) - 6\gamma_a^2\eta_1 + \gamma_a\mu_0, \quad \text{(B5)}$$
$$\alpha_4 = \gamma_a^4 - 4\gamma_a^3\eta_1 + \gamma_a^2\mu_2 - \gamma_a\mu_3 + 2\,\Re_+\Re_-\eta_5, \quad \text{(B6)}$$
$$\alpha_5 = 2g^4\gamma_a - J^4\eta_1 + g^2\mu_5 - 2J^2\mu_6 - \eta_4\mu_7, \quad \text{(B7)}$$
$$\alpha_6 = g^4\eta_4 + \eta_2\mu_8 - g^2\mu_9, \quad \text{(B8)}$$

with

$$\eta_1 = \Re_+ + \Re_-, \quad \eta_2 = \Re_+\Re_- - \Im_+\Im_-,$$
$$\eta_3 = \Im_+ - \Im_-, \quad \eta_4 = \gamma_a^2 + \Delta_a^2,$$
$$\eta_5 = J^2 + \Delta_a^2, \quad \mu_0 = 6g^2 + 4(\eta_5 + \eta_2),$$
$$\mu_1 = g^4 + 2g^2J^2 + J^4 - 2J^2\Delta_a^2 + \Delta_a^4,$$
$$\mu_2 = 6(g^2 + \eta_2) + 2\eta_5, \quad \mu_3 = \left(4\Delta_a^2 + 3g^2 + 4J^4\right)\eta_1,$$
$$\mu_4 = 2\,\Im_+\Im_-\eta_5 - g^2\Delta_a(2\Delta_a - \eta_3),$$
$$\mu_5 = 2\gamma_a^3 + J^2(2\gamma_a - \eta_1) - \left(3\gamma_a^2 + \Delta_a^2\right) \times \eta_1 + 2\gamma_a\Delta_a(\Delta_a - \Im_+ + \Im_-),$$
$$\mu_6 = \eta_4\eta_1 - 2\gamma_a\eta_2, \quad \mu_7 = \eta_4\eta_1 - 4\gamma_a\eta_2,$$
$$\mu_8 = J^4 + 2J^2\left(\gamma_a^2 - \Delta_a^2\right) + \eta_4^2,$$
$$\mu_9 = \eta_4(\gamma_a\eta_1 + \Delta_a\eta_3) + J^2(\gamma_a\eta_1 - \Delta_a\eta_3).$$

Note that for simplicity, here we have assumed that the parameters of the two cavity modes are completely consistent, i.e., $\gamma_{a_1} = \gamma_{a_2} = \gamma_a$ and $\Delta_{a_1} = \Delta_{a_2} = \Delta_a$ (all numerical results in the main text are also based on this assumption). Based on coefficient α_k, one can construct six Hurwitz matrices, where the dimension of the kth matrix is $k \times k$ ($1 \leqslant k \leqslant 6$), the corresponding matrix elements are determined by the following conditions [75]:

$$\mathfrak{H}_{ij}^k = \begin{cases} 0, & 2i - j < 0 \quad \text{or} \quad 2i - j > k \\ \alpha_{2i-j}, & \text{otherwise} \end{cases} \quad \text{(B9)}$$

where $1 \leqslant i, j \leqslant k$. For example, when $k = 1$ and 3, we can easily obtain by Eq. (B9)

$$\mathfrak{H}^1 = [\alpha_1], \quad \mathfrak{H}^3 = \begin{bmatrix} \alpha_1 & 1 & 0 \\ \alpha_3 & \alpha_2 & \alpha_1 \\ 0 & 0 & \alpha_3 \end{bmatrix}. \quad \text{(B10)}$$

The stability condition of the system is that all the determinants of Hurwitz matrices are positive, i.e.,

$$\forall \det\left[\mathfrak{H}^k\right] > 0 \text{ holds}, \ 1 \leqslant k \leqslant 6. \quad \text{(B11)}$$

Based on Eq. (B11), the following conditions are obtained, i.e.,

$$\alpha_i > 0 \ (1 \leqslant i, j \leqslant k); \ \alpha_1\alpha_2 > \alpha_3, \quad \text{(B12)}$$

$$\alpha_1\alpha_2\alpha_3 > \alpha_3^2 + \alpha_1^2\alpha_4; \ T_1 > T_2; \ T_3 > T_4, \quad \text{(B13)}$$

with

$$T_1 = (\alpha_1\alpha_4 - \alpha_5)\left(\alpha_1\alpha_2\alpha_3 - \alpha_3^2 - \alpha_1^2\alpha_4\right),$$
$$T_2 = \alpha_1\alpha_5^2 + \alpha_5(\alpha_1\alpha_2 - \alpha_3)^2,$$
$$T_3 = \alpha_1^2\alpha_6(2\alpha_2\alpha_5 + \alpha_3\alpha_4) + \alpha_3^3\alpha_6 + \alpha_1\alpha_2\alpha_3\alpha_4\alpha_5 + \alpha_5^2(2\alpha_1\alpha_4 + \alpha_2\alpha_3),$$
$$T_4 = \alpha_1^2\left(\alpha_1\alpha_6^2 + \alpha_4^2\alpha_5\right) + \alpha_5^3 + \alpha_4\alpha_5\alpha_3^2 + \alpha_1\left(\alpha_2\alpha_6\alpha_3^2 + 3\alpha_3\alpha_5\alpha_6 + \alpha_2^2\alpha_5^2\right).$$

Equations (B12) and (B13) ensure the stability of the driven-dissipative double-cavity-magnon system.

APPENDIX C: PARAMETER ESTIMATION THEORY FOR QUANTUM GAUSSIAN STATES

For the convenience of the reader, here we introduce the main aspects of the Gaussian parameter estimation framework based on the discussed cavity-magnon system.

1. Quantum Fisher information for Gaussian states

Known the first moment $\langle\hat{\mathbf{R}}_0\rangle := [\langle\hat{Q}_{a_1}\rangle, \langle\hat{P}_{a_1}\rangle, \langle\hat{Q}_{a_2}\rangle, \langle\hat{P}_{a_2}\rangle, \langle\hat{Q}_m\rangle, \langle\hat{P}_m\rangle]^{\mathrm{T}}$ and steady-state covariance matrix $\mathcal{V}$, the QFI of the global state reads as [61–64]

$$\mathcal{F}_g = 2\,\mathrm{vec}[\partial_g\mathcal{V}]^\dagger\mathfrak{M}^{-1}\mathrm{vec}[\partial_g\mathcal{V}] + \partial_g\langle\hat{\mathbf{R}}_\mathbf{0}\rangle^{\mathrm{T}}\mathcal{V}^{-1}\partial_g\langle\hat{\mathbf{R}}_\mathbf{0}\rangle, \quad \text{(C1)}$$

where $\mathfrak{M} = (4\mathcal{V}^\dagger \otimes \mathcal{V} + \Xi \otimes \Xi)$; $\mathrm{vec}[\mathfrak{G}]$ denotes the vectorization of a matrix $\mathfrak{G}$ (n dimension), which is defined as $\mathrm{vec}[\mathfrak{G}] := [\mathfrak{G}(:,1)^{\mathrm{T}}, \mathfrak{G}(:,2)^{\mathrm{T}}, \cdots, \mathfrak{G}(:,n)^{\mathrm{T}}]^{\mathrm{T}}$, and $\mathfrak{G}(:,n)$ being the nth column of $\mathfrak{G}$. One can see that its first term is the contribution owing to the dependence of the second moment on g, while the second term is the contribution originating from the dependence of the first moment on g. In the process of numerical simulation, in order to achieve sufficient numerical accuracy, the first-order derivative of any g-dependent function is treated by the Lagrange interpolation method [76,77]. To find the optimal subsystem for estimating g, we introduce the QFI for each subsystem

$$\mathcal{F}_g^i = 2\,\mathrm{vec}[\partial_g L_i]^\dagger M_i^{-1}\mathrm{vec}[\partial_g L_i] + \partial_g\langle\hat{d}_i\rangle^{\mathrm{T}}L_i^{-1}\partial_g\langle\hat{d}_i\rangle, \quad \text{(C2)}$$

with

$$M_i = (4L_i^\dagger \otimes L_i + \Lambda \otimes \Lambda), \quad \langle\hat{d}_i\rangle = [\langle\hat{Q}_i\rangle, \langle\hat{P}_i\rangle]^{\mathrm{T}}, \quad \text{(C3)}$$

where $i = a_1$, a_2, and m; $\mathcal{F}_g^i$ and $\langle\hat{d}_i\rangle$ correspond to the QFI and displacement vector for mode i, respectively.

2. Classical Fisher information for Gaussian states

a. Homodyne detection

For homodyne detection, the corresponding CFI is [63]

$$F^{k}_{g,\mathrm{Ho}} = \frac{1}{2\mathcal{V}^2_{kk}}[2\mathcal{V}_{kk}(\partial_g\langle\hat{\mathbf{R}}_0\rangle_k)^2 + (\partial_g\mathcal{V}_{kk})^2], \tag{C4}$$

where $\langle\hat{\mathbf{R}}_0\rangle_k$ being the steady-state value of the selected quadrature operator ($k = 1 \sim 6$, corresponds sequentially to $\hat{Q}_{a_1}, \hat{P}_{a_1}, \hat{Q}_{a_2}, \hat{P}_{a_2}, \hat{Q}_m, \hat{P}_m$); $\mathcal{V}_{kk}$ being the diagonal element of the covariance matrix $\mathcal{V}$. For instance, we have that $\langle\hat{\mathbf{R}}_0\rangle_4 = \langle\hat{P}_{a_2}\rangle$ and $\mathcal{V}_{44} = \langle[\delta\hat{P}_{a_2}(\infty)]^2\rangle$ for $k = 4$, i.e., performing homodyne detection on the phase quadrature of cavity mode 2.

b. Heterodyne detection

For heterodyne detection, the corresponding CFI reads as [63]

$$F^{i}_{g,\mathrm{He}} = \tfrac{1}{2}\mathrm{Tr}[(\aleph^{-1}\partial_g\aleph)^2] + \partial_g\langle\hat{d}_i\rangle^{\mathrm{T}}\aleph^{-1}\partial_g\langle\hat{d}_i\rangle, \tag{C5}$$

where $\aleph_i = L_i + \mathbb{1}_2$; $\langle\hat{d}_i\rangle$ and L_i are the first moment and the covariance matrix of the selected mode, respectively. Particularly, $\mathbb{1}_2$ is a 2×2 identity matrix, which represents the added noise in L_i stems from the simultaneous detection of the conjugated quadratures. For example, if heterodyne detection is considered for the cavity mode 2, they take the form, respectively, of $\langle\hat{d}_i\rangle = [\langle\hat{Q}_{a_2}\rangle, \langle\hat{P}_{a_2}\rangle]^{\mathrm{T}}$ and $L_i = L_{a_2}$.

c. Optimal Gaussian measurement

More generally, the CFIs obtained by performing arbitrary Gaussian measurements on Gaussian states can be uniformly expressed as [78]

$$F^{\mathrm{GM}}_g\big(\mathbf{d},\boldsymbol{\sigma};\boldsymbol{\sigma}^M_{\mathrm{GS}}\big) = \partial_g\mathbf{d}^{\mathrm{T}}\big(\boldsymbol{\sigma}+\boldsymbol{\sigma}^M_{\mathrm{GS}}\big)^{-1}\partial_g\mathbf{d} + \tfrac{1}{2}\mathrm{Tr}\Big[\Big[\big(\boldsymbol{\sigma}+\boldsymbol{\sigma}^M_{\mathrm{GS}}\big)^{-1}\partial_g\boldsymbol{\sigma}\Big]^2\Big], \tag{C6}$$

where $\mathbf{d}$ and $\boldsymbol{\sigma}$ are the first moment and covariance matrix of the observed mode, respectively; $\boldsymbol{\sigma}^M_{\mathrm{GS}}$ is the covariance matrix of Gaussian measurement operator.

When $\mathbf{d}$ and $\boldsymbol{\sigma}$ of the observation mode are fixed, the optimal $\boldsymbol{\sigma}^M_{\mathrm{GS}}$ must be found to maximize F^{GM}_g. However, this is in general a notoriously difficult task to analytically obtain the optimal $\boldsymbol{\sigma}^M_{\mathrm{GS}}$. The main obstacle stems from the objective function $F^{\mathrm{OGM}}_g = \underset{\boldsymbol{\sigma}^M_{GS}}{\mathrm{Max}}\{F^{\mathrm{GM}}_g\}$ is a nonlinear function of the measurement covariance matrix $\boldsymbol{\sigma}^M_{\mathrm{GS}}$. Note also that the quantum state to which the covariance matrix of the optimal Gaussian measurement belongs must be a pure state, which leads to $\boldsymbol{\sigma}^M_{\mathrm{GS}} = \boldsymbol{\sigma}^M_{\max} \equiv S^M(S^M)^{\mathrm{T}}$ always holding [58]. Here S^M is a symplectic transformation, satisfying the symmetric constraint condition $S^M\Lambda(S^M)^{\mathrm{T}} = \Lambda$. In this scenario, finding F^{OGM}_g is transformed into the following semidefinite programming (SDP) problem [78]:

$$F^{\mathrm{OGM}}_g := \underset{S^M}{\mathrm{Max}}\big\{F^{\mathrm{GM}}_g(\mathbf{d},\boldsymbol{\sigma};S^M(S^M)^{\mathrm{T}})\big\},$$
$$\text{s.t. } \Lambda = S^M\Lambda(S^M)^{\mathrm{T}}. \tag{C7}$$

Currently, we are still concerned with performing measurements on single-mode Gaussian states.

APPENDIX D: NORMAL MODE PICTURE

The effective Hamiltonian of the double-cavity-magnon system is

$$\begin{aligned}\hat{H}_{1,\mathrm{eff}} =\ & \Delta_1\delta\hat{a}_1^\dagger\delta\hat{a}_1 + \Delta_2\delta\hat{a}_2^\dagger\delta\hat{a}_2 + \Delta_{\mathrm{eff}}\delta\hat{m}^\dagger\delta\hat{m}\\ & + K[\langle\hat{m}\rangle^2\delta\hat{m}^\dagger\delta\hat{m}^\dagger + \langle\hat{m}\rangle^{*^2}\delta\hat{m}\delta\hat{m}]\\ & + J(\delta\hat{a}_1^\dagger\delta\hat{a}_2 + \delta\hat{a}_1\delta\hat{a}_2^\dagger) + g(\delta\hat{a}_2^\dagger\delta\hat{m} + \delta\hat{a}_2\delta\hat{m}^\dagger).\end{aligned} \tag{D1}$$

Based on the above equation, one can clearly see that only cavity mode 2 and the magnon are coupled via beam-splitter-like interaction while the magnon is subject to single-mode squeezing. However, in the normal mode picture, the two interactions take on a different form.

Introducing Bogoliubov transformation [79]

$$\hat{M} := \alpha\delta\hat{m} - \beta^*\delta\hat{m}^\dagger, \tag{D2a}$$
$$\hat{M}^\dagger := \alpha^*\delta\hat{m}^\dagger - \beta\delta\hat{m}, \tag{D2b}$$

with

$$\alpha = \sqrt{(\Delta_{\mathrm{eff}}/\mathcal{E}+1)/2}, \quad \beta e^{i\phi} = -\sqrt{(\Delta_{\mathrm{eff}}/\mathcal{E}-1)/2},$$
$$\mathcal{E} = \sqrt{\Delta^2_{\mathrm{eff}} - 4|\langle\hat{m}\rangle|^4K^2}, \quad \phi = \arctan(\mathcal{I}/\mathcal{R}),$$

where $\mathcal{I} = \mathrm{Im}(2K\langle\hat{m}\rangle^2)$ and $\mathcal{R} = \mathrm{Re}(2K\langle\hat{m}\rangle^2)$ quantified the magnetocrystalline anisotropy of YIG sphere. Substituting Eqs. (D2) into Eq. (D1), $\hat{H}_{1,\mathrm{eff}}$ can be written as

$$\begin{aligned}\hat{\mathcal{H}}_{1,\mathrm{eff}} =\ & \Delta_1\delta\hat{a}_1^\dagger\delta\hat{a}_1 + \Delta_2\delta\hat{a}_2^\dagger\delta\hat{a}_2 + \mathcal{E}\hat{M}^\dagger\hat{M}\\ & + g[(\beta\hat{M} + \alpha\hat{M}^\dagger)\delta\hat{a}_2 + (\beta^*\hat{M}^\dagger + \alpha^*\hat{M})\delta\hat{a}_2^\dagger]\\ & + J(\delta\hat{a}_1^\dagger\delta\hat{a}_2 + \delta\hat{a}_1\delta\hat{a}_2^\dagger),\end{aligned} \tag{D3}$$

where $g(\beta\hat{M}\delta\hat{a}_2 + \beta^*\hat{M}^\dagger\delta\hat{a}_2^\dagger)$ being the squeezinglike coupling, resulting in the entanglement between the normal magnon mode $\hat{M}$ and the cavity mode 2. Notice also that Kerr coefficient $K = 0$ makes $\beta = 0$ owing to $\Delta_{\mathrm{eff}} = \mathcal{E}$, leading to the squeezinglike coupling disappear. This indicates that the magnetocrystalline anisotropy is the key to inducing the entanglement between the magnon and the cavity mode 2.

In order to clearly show the two cavity-magnon interactions corresponding to the double-peak structure in Fig. 5(a), we further introduce the following transformation, i.e.,

$$\hat{A}_+ := f\delta\hat{a}_1 - h\delta\hat{a}_2, \tag{D4a}$$
$$\hat{A}_- := h\delta\hat{a}_1 + f\delta\hat{a}_2. \tag{D4b}$$

Substituting the above formula into Eq. (D1), we can obtain

$$\begin{aligned}\hat{H}_{2,\mathrm{eff}} =\ & \Delta_{\mathrm{eff}}\delta\hat{m}^\dagger\delta\hat{m} + K[\langle\hat{m}\rangle^2\delta\hat{m}^\dagger\delta\hat{m}^\dagger + \langle\hat{m}\rangle^{*^2}\delta\hat{m}\delta\hat{m}]\\ & + \omega_+\hat{A}_+^\dagger\hat{A}_+ + \omega_-\hat{A}_-^\dagger\hat{A}_- + G_+(\delta\hat{m}\hat{A}_+^\dagger + \delta\hat{m}^\dagger\hat{A}_+)\\ & + G_-(\delta\hat{m}\hat{A}_-^\dagger + \delta\hat{m}^\dagger\hat{A}_-),\end{aligned} \tag{D5}$$

where $\omega_\pm$ refers to the resonance frequency of hybridized cavity modes; $G_\pm$ is the coupling strength between the

hybridized cavity modes and the magnons. Their specific forms
are

$$G_+ = -gh, \quad G_- = fg, \tag{D6}$$

$$\omega_\pm = \tfrac{1}{2}[(\Delta_1 + \Delta_2) \pm \sqrt{(\Delta_1 - \Delta_2)^2 + 4J^2}], \tag{D7}$$

with $f = |\omega_- - \Delta_1|/\sqrt{(\omega_- - \Delta_1)^2 + J^2}$ and $h = Jf/(\omega_- - \Delta_1)$, in which $f^2 + h^2 = 1$.

Further, Eq. (D3) can be rewritten as

$$\begin{aligned}\hat{\mathcal{H}}_{2,\text{eff}} = {} & \omega_+\hat{A}_+^\dagger\hat{A}_+ + \omega_-\hat{A}_-^\dagger\hat{A}_- + \mathcal{E}\hat{M}^\dagger\hat{M} \\ & + G_+[(\beta\hat{M} + \alpha\hat{M}^\dagger)\hat{A}_+ + (\beta^*\hat{M}^\dagger + \alpha^*\hat{M})\hat{A}_+^\dagger] \\ & + G_-[(\beta\hat{M} + \alpha\hat{M}^\dagger)\hat{A}_- + (\beta^*\hat{M}^\dagger + \alpha^*\hat{M})\hat{A}_-^\dagger].\end{aligned} \tag{D8}$$

From Eq. (D8), we can clearly see that the interaction between the magnon and the two cavity modes is essentially equivalent to that between the normal magnon mode $\hat{M}$ and the two hybrid cavity modes ($\hat{A}_+$ and $\hat{A}_-$).

[1] P. Meystre and M. Sargent, *Elements of Quantum Optics* (Springer, New York, 2007).

[2] M. O. Scully and M. S. Zubairy, *Quantum Optics* (Cambridge University Press, Cambridge, 1999).

[3] N. Papasimakis, V. Fedotov, V. Savinov, T. Raybould, and N. Zheludev, Electromagnetic toroidal excitations in matter and free space, Nat. Mater. **15**, 263 (2016).

[4] B. Bhoi and S.-K. Kim, Photon-magnon coupling: Historical perspective, status, and future directions, Solid State Phys. **70**, 1 (2019).

[5] H. Yuan, Y. Cao, A. Kamra, R. A. Duine, and P. Yan, Quantum magnonics: When magnon spintronics meets quantum information science, Phys. Rep. **965**, 1 (2022).

[6] B. Z. Rameshti, S. V. Kusminskiy, J. A. Haigh, K. Usami, D. Lachance-Quirion, Y. Nakamura, C.-M. Hu, H. X. Tang, G. E. Bauer, and Y. M. Blanter, Cavity magnonics, Phys. Rep. **979**, 1 (2022).

[7] X. Zhang, C.-L. Zou, L. Jiang, and H. X. Tang, Cavity magnomechanics, Sci. Adv. **2**, e1501286 (2016).

[8] H. Huebl, C. W. Zollitsch, J. Lotze, F. Hocke, M. Greifenstein, A. Marx, R. Gross, and S. T. B. Goennenwein, High cooperativity in coupled microwave resonator ferrimagnetic insulator hybrids, Phys. Rev. Lett. **111**, 127003 (2013).

[9] X. Zhang, C.-L. Zou, L. Jiang, and H. X. Tang, Strongly coupled magnons and cavity microwave photons, Phys. Rev. Lett. **113**, 156401 (2014).

[10] J. Li, S.-Y. Zhu, and G. S. Agarwal, Magnon-photon-phonon entanglement in cavity magnomechanics, Phys. Rev. Lett. **121**, 203601 (2018).

[11] J. Li and S.-Y. Zhu, Entangling two magnon modes via magnetostrictive interaction, New J. Phys. **21**, 085001 (2019).

[12] Z. Zhang, M. O. Scully, and G. S. Agarwal, Quantum entanglement between two magnon modes via kerr nonlinearity driven far from equilibrium, Phys. Rev. Res. **1**, 023021 (2019).

[13] V. Azimi Mousolou, Y. Liu, A. Bergman, A. Delin, O. Eriksson, M. Pereiro, D. Thonig, and E. Sjöqvist, Magnon-magnon entanglement and its quantification via a microwave cavity, Phys. Rev. B **104**, 224302 (2021).

[14] H.-J. Cheng, S.-J. Zhou, J.-X. Peng, A. Kundu, H.-X. Li, L. Jin, and X.-L. Feng, Tripartite entanglement in a Laguerre–Gaussian rotational-cavity system with an yttrium iron garnet sphere, J. Opt. Soc. Am. B **38**, 285 (2021).

[15] W.-L. Xu, X.-F. Liu, Y. Sun, Y.-P. Gao, T.-J. Wang, and C. Wang, Magnon-induced chaos in an optical pt-symmetric resonator, Phys. Rev. E **101**, 012205 (2020).

[16] Z.-X. Liu, C. You, B. Wang, H. Xiong, and Y. Wu, Phase-mediated magnon chaos-order transition in cavity optomagnonics, Opt. Lett. **44**, 507 (2019).

[17] Z. R. Yan, C. H. Wan, and X. F. Han, Magnon blocking effect in an antiferromagnet-spaced magnon junction, Phys. Rev. Appl. **14**, 044053 (2020).

[18] Z.-X. Liu, H. Xiong, and Y. Wu, Magnon blockade in a hybrid ferromagnet-superconductor quantum system, Phys. Rev. B **100**, 134421 (2019).

[19] K. Ullah, M. T. Naseem, and Ö. E. Müstecaplıoğlu, Tunable multiwindow magnomechanically induced transparency, fano resonances, and slow-to-fast light conversion, Phys. Rev. A **102**, 033721 (2020).

[20] C. Kong, H. Xiong, and Y. Wu, Magnon-induced nonreciprocity based on the magnon Kerr effect, Phys. Rev. Appl. **12**, 034001 (2019).

[21] C. Zhao, Z. Yang, R. Peng, J. Yang, C. Li, and L. Zhou, Dissipative-coupling-induced transparency and high-order sidebands with kerr nonlinearity in a cavity-magnonics system, Phys. Rev. Appl. **18**, 044074 (2022).

[22] Y.-P. Wang, G.-Q. Zhang, D. Zhang, T.-F. Li, C.-M. Hu, and J. Q. You, Bistability of cavity magnon polaritons, Phys. Rev. Lett. **120**, 057202 (2018).

[23] H. Pan, Y. Yang, Z. H. An, and C.-M. Hu, Bistability in dissipatively coupled cavity magnonics, Phys. Rev. B **106**, 054425 (2022).

[24] Z.-B. Yang, H. Jin, J.-W. Jin, J.-Y. Liu, H.-Y. Liu, and R.-C. Yang, Bistability of squeezing and entanglement in cavity magnonics, Phys. Rev. Res. **3**, 023126 (2021).

[25] Y.-P. Wang, G.-Q. Zhang, D. Zhang, X.-Q. Luo, W. Xiong, S.-P. Wang, T.-F. Li, C.-M. Hu, and J. Q. You, Magnon kerr effect in a strongly coupled cavity-magnon system, Phys. Rev. B **94**, 224410 (2016).

[26] G. Zhang, Y. Wang, and J. You, Theory of the magnon kerr effect in cavity magnonics, Sci. China Phys. Mech. Astron. **62**, 987511 (2019).

[27] A. Prabhakar and D. D. Stancil, *Spin Waves: Theory and Applications* (Springer, Berlin, 2009), Vol. 5.

[28] C. W. Helstrom, Quantum detection and estimation theory, J. Stat. Phys. **1**, 231 (1969).

[29] J. Liu, H. Yuan, X.-M. Lu, and X. Wang, Quantum fisher information matrix and multiparameter estimation, J. Phys. A: Math. Theor. **53**, 023001 (2020).

[30] M. G. Paris, Quantum estimation for quantum technology, Int. J. Quantum Inf. **07**, 125 (2009).

[31] J. Z. Bernád, C. Sanavio, and A. Xuereb, Optimal estimation of matter-field coupling strength in the dipole approximation, Phys. Rev. A **99**, 062106 (2019).

[32] H. Chen and H. Yuan, Optimal joint estimation of multiple Rabi frequencies, Phys. Rev. A **99**, 032122 (2019).

[33] D. Burgarth, K. Maruyama, and F. Nori, Coupling strength estimation for spin chains despite restricted access, Phys. Rev. A **79**, 020305(R) (2009).

[34] M. C. Romano, M. Thiel, J. Kurths, and C. Grebogi, Estimation of the direction of the coupling by conditional probabilities of recurrence, Phys. Rev. E **76**, 036211 (2007).

[35] D. Xie and C. Xu, Quantum estimation of tripartite coupling in spin-magnon-mechanical hybrid systems, arXiv:2305.12435.

[36] L. Qiao, J.-X. Peng, B. Zhu, W. Zhang, and K. Zhang, Optimal initial states for quantum parameter estimation based on jaynes–cummings model, Chin. Opt. Lett. **21**, 102701 (2023).

[37] S. Qvarfort, A. D. K. Plato, D. E. Bruschi, F. Schneiter, D. Braun, A. Serafini, and D. Rätzel, Optimal estimation of time-dependent gravitational fields with quantum optomechanical systems, Phys. Rev. Res. **3**, 013159 (2021).

[38] V. Montenegro, M. G. Genoni, A. Bayat, and M. G. A. Paris, Probing of nonlinear hybrid optomechanical systems via partial accessibility, Phys. Rev. Res. **4**, 033036 (2022).

[39] J. Z. Bernád, C. Sanavio, and A. Xuereb, Optimal estimation of the optomechanical coupling strength, Phys. Rev. A **97**, 063821 (2018).

[40] F. Schneiter, S. Qvarfort, A. Serafini, A. Xuereb, D. Braun, D. Rätzel, and D. E. Bruschi, Optimal estimation with quantum optomechanical systems in the nonlinear regime, Phys. Rev. A **101**, 033834 (2020).

[41] C. Sanavio, J. Z. Bernád, and A. Xuereb, Fisher-information-based estimation of optomechanical coupling strengths, Phys. Rev. A **102**, 013508 (2020).

[42] S. Carrasco and M. Orszag, Estimation of an optomechanical parameter via weak-value amplification, Phys. Rev. A **105**, 043508 (2022).

[43] K. Sala, T. Doicin, A. D. Armour, and T. Tufarelli, Quantum estimation of coupling strengths in driven-dissipative optomechanics, Phys. Rev. A **104**, 033508 (2021).

[44] Y.-M. Liu, C.-H. Bai, D.-Y. Wang, T. Wang, M.-H. Zheng, H.-F. Wang, A.-D. Zhu, and S. Zhang, Ground-state cooling of rotating mirror in double-laguerre-gaussian-cavity with atomic ensemble, Opt. Express **26**, 6143 (2018).

[45] W.-X. Yang, A.-X. Chen, X.-T. Xie, and L. Ni, Enhanced generation of higher-order sidebands in a single-quantum-dot–cavity system coupled to a $\mathcal{PT}$-symmetric double cavity, Phys. Rev. A **96**, 013802 (2017).

[46] C. Tchodimou, P. Djorwe, and S. G. Nana Engo, Distant entanglement enhanced in $\mathcal{PT}$-symmetric optomechanics, Phys. Rev. A **96**, 033856 (2017).

[47] Z.-B. Yang, Y. Ming, R.-C. Yang, and H.-Y. Liu, Asymmetric transmission and entanglement in a double-cavity magnomechanical system, J, Opt. Soc. Am. B **40**, 822 (2023).

[48] Y.-T. Chen, L. Du, Y. Zhang, and J.-H. Wu, Perfect transfer of enhanced entanglement and asymmetric steering in a cavity-magnomechanical system, Phys. Rev. A **103**, 053712 (2021).

[49] A. Sohail, R. Ahmed, J.-X. Peng, A. Shahzad, and S. Singh, Enhanced entanglement via magnon squeezing in a two-cavity magnomechanical system, J. Opt. Soc. Am. B **40**, 1359 (2023).

[50] A. Hidki, A. Lakhfif, J. El Qars, and M. Nassik, Quantifying quantum correlations in a double cavity–magnon system, Eur. Phys. J. D **76**, 64 (2022).

[51] C. Zhao, R. Peng, Z. Yang, S. Chao, C. Li, Z. Wang, and L. Zhou, Nonreciprocal amplification in a cavity magnonics system, Phys. Rev. A **105**, 023709 (2022).

[52] Y. Qin, S.-C. Li, K. Li, and J.-J. Song, Controllable quantum phase transition in a double-cavity magnonic system, Phys. Rev. B **106**, 054419 (2022).

[53] R. A. Fisher, Theory of statistical estimation, in *Mathematical Proceedings of the Cambridge Philosophical Society* (Cambridge University Press, Cambridge, 1925), Vol. 22, pp. 700–725.

[54] S. L. Braunstein and C. M. Caves, Statistical distance and the geometry of quantum states, Phys. Rev. Lett. **72**, 3439 (1994).

[55] Y. Chen, Y.-L. Zhang, Z. Shen, C.-L. Zou, G.-C. Guo, and C.-H. Dong, Synthetic gauge fields in a single optomechanical resonator, Phys. Rev. Lett. **126**, 123603 (2021).

[56] H.-P. Breuer and F. Petruccione, *The Theory of Open Quantum Systems* (Oxford University Press, New York, 2002).

[57] M. Aspelmeyer, T. J. Kippenberg, and F. Marquardt, Cavity optomechanics, Rev. Mod. Phys. **86**, 1391 (2014).

[58] A. Serafini, *Quantum Continuous Variables: A Primer of Theoretical Methods* (CRC Press, Boca Raton, FL, 2023).

[59] I. Wilson-Rae, N. Nooshi, J. Dobrindt, T. J. Kippenberg, and W. Zwerger, Cavity-assisted backaction cooling of mechanical resonators, New J. Phys. **10**, 095007 (2008).

[60] R. R. Puri, *Mathematical Methods of Quantum Optics*, Vol. 79 (Springer, Berlin, 2001).

[61] L. Bakmou, M. Daoud *et al.*, Multiparameter quantum estimation theory in quantum Gaussian states, J. Phys. A: Math. Theor. **53**, 385301 (2020).

[62] O. Pinel, J. Fade, D. Braun, P. Jian, N. Treps, and C. Fabre, Ultimate sensitivity of precision measurements with intense Gaussian quantum light: A multimodal approach, Phys. Rev. A **85**, 010101(R) (2012).

[63] A. Monras, Phase space formalism for quantum estimation of gaussian states, arXiv:1303.3682.

[64] D. Šafránek, Estimation of Gaussian quantum states, J. Phys. A: Math. Theor. **52**, 035304 (2018).

[65] C. Oh, C. Lee, C. Rockstuhl, H. Jeong, J. Kim, H. Nha, and S.-Y. Lee, Optimal Gaussian measurements for phase estimation in single-mode gaussian metrology, npj Quantum Inf. **5**, 10 (2019).

[66] L. J. Fiderer and D. Braun, Quantum metrology with quantum-chaotic sensors, Nat. Commun. **9**, 1351 (2018).

[67] M. Yu, D. Li, J. Wang, Y. Chu, P. Yang, M. Gong, N. Goldman, and J. Cai, Experimental estimation of the quantum fisher information from randomized measurements, Phys. Rev. Res. **3**, 043122 (2021).

[68] X. Zhang, X.-M. Lu, J. Liu, W. Ding, and X. Wang, Direct measurement of quantum fisher information, Phys. Rev. A **107**, 012414 (2023).

[69] M. Valeri, V. Cimini, S. Piacentini, F. Ceccarelli, E. Polino, F. Hoch, G. Bizzarri, G. Corrielli, N. Spagnolo, R. Osellame *et al.*, Experimental multiparameter quantum metrology in adaptive regime, Phys. Rev. Res. **5**, 013138 (2023).

[70] M. Yu, Y. Liu, P. Yang, M. Gong, Q. Cao, S. Zhang, H. Liu, M. Heyl, T. Ozawa, N. Goldman *et al.*, Quantum fisher information

measurement and verification of the quantum cramér–rao bound in a solid-state qubit, npj Quantum Inf. **8**, 56 (2022).

[71] S. Blundell, *Magnetism in Condensed Matter* (Oxford University Press, Oxford, 2001).

[72] O. O. Soykal and M. E. Flatté, Strong field interactions between a nanomagnet and a photonic cavity, Phys. Rev. Lett. **104**, 077202 (2010).

[73] T. Holstein and H. Primakoff, Field dependence of the intrinsic domain magnetization of a ferromagnet, Phys. Rev. **58**, 1098 (1940).

[74] E. X. DeJesus and C. Kaufman, Routh-hurwitz criterion in the examination of eigenvalues of a system of nonlinear ordinary differential equations, Phys. Rev. A **35**, 5288 (1987).

[75] Y.-F. Jiao, S.-D. Zhang, Y.-L. Zhang, A. Miranowicz, L.-M. Kuang, and H. Jing, Nonreciprocal optomechanical entanglement against backscattering losses, Phys. Rev. Lett. **125**, 143605 (2020).

[76] Y.-D. Sha and W. Wu, Continuous-variable quantum sensing of a dissipative reservoir, Phys. Rev. Res. **4**, 023169 (2022).

[77] Z.-Z. Zhang and W. Wu, Effects of counter-rotating-wave terms on the noisy frequency estimation, Phys. Rev. A **105**, 043706 (2022).

[78] M. F. Cenni, L. Lami, A. Acin, and M. Mehboudi, Thermometry of gaussian quantum systems using gaussian measurements, Quantum **6**, 743 (2022).

[79] A. L. Fetter and J. D. Walecka, *Quantum Theory of Many-particle Systems* (Dover, New York, 2012).